Heterogeneous Reactivity of Gaseous Nitric Acid on Al_2O_3, $CaCO_3$, and Atmospheric Dust Samples: A Knudsen Cell Study

F. Hanisch and J. N. Crowley*

Max-Planck-Institut für Chemie, Division of Atmospheric Chemistry, Postfach 3060, 55020 Mainz, Germany

Received: March 31, 2000; In Final Form: October 24, 2000

The heterogeneous reaction between HNO_3 and various authentic and synthetic mineral dust/mineral oxide surfaces has been investigated using a low-pressure Knudsen reactor operating at 298 K. The surfaces used were Saharan dust from Cape Verde, Arizona dust, $CaCO_3$, and Al_2O_3. In all cases, a large irreversible uptake was observed. An uptake coefficient of $\gamma = (11 \pm 3) \times 10^{-2}$ was determined for Saharan dust, and $\gamma = (6 \pm 1.5) \times 10^{-2}$ was obtained for Arizona dust. The uptake coefficients for HNO_3 on heated $CaCO_3$ and on unheated $CaCO_3$ are given by $\gamma = (10 \pm 2.5) \times 10^{-2}$ and $(18 \pm 4.5) \times 10^{-2}$, respectively, and are in good agreement with previous results. CO_2 and H_2O were formed as gas-phase products. Measurements of the uptake coefficient of HNO_3 on grain-size selected samples of Al_2O_3, $\gamma = (13 \pm 3.3) \times 10^{-2}$, and systematic variation of sample mass enabled us to show that the geometrical surface area of the dust sample is appropriate for calculation of uptake coefficients in these experiments. The high reactivity of HNO_3 toward dust samples highlights the potentially important role of mineral dust in redistributing nitrate from the gaseous to the particulate phase and modifying tropospheric photochemical oxidation cycles.

1. Introduction

About 33% of the earth's land surface is arid and a potential source region for atmospheric mineral aerosol.[1] Mineral aerosol is a general expression for fine particles of crustal origin that are generated by wind erosion, and which consist mostly of silica and silicate minerals. Mineral aerosol is uplifted into the atmosphere by strong surface winds that travel behind cold frontal systems.[2] Current estimates of annual dust emissions are in the range of 1000−3000 Tg/year.[3] The major source areas of the world are situated in a broad band that extends from the west coast of North Africa across the Arabian Peninsula to central Asia (see, e.g., ref 4). Particles smaller than 10 μm have atmospheric lifetimes of weeks,[4] and mineral aerosol may be transported over thousands of kilometers enabling Saharan dust to be transported to, e.g., Florida and Barbados[5] and central Asian dust to the northern Pacific islands.[6] Globally, the most important minerals of the clay fraction (<2 μm) transported in dust storms are illite, kaolinite, chlorite, and montmorillonite/smectite,[7,4] whereas coarser particles mainly consist of quartz, feldspars, and carbonates.[8]

In the past, mineral aerosol has been taken into consideration by atmospheric scientists mainly in connection with the radiation budget of the earth. Its properties with respect to absorption and scattering of solar and terrestrial radiation and its suitability as cloud condensation nuclei have been subject of investigation. However, recent modeling studies[9,10] have predicted that mineral aerosol could also have a significant influence on atmospheric chemistry by promoting heterogeneous reactions. At a loading of 100 μg/m^3, mineral aerosol has been predicted to reduce [NO_y] (NO_y: total reactive nitrogen = $NOx + HNO_3 + HONO + NO_3 + 2N_2O_5 + HNO_4 + PAN + RONO_2 + ROONO_2 + RNO_2$, where $NOx = NO + NO_2$) by 56% during daytime periods and by 98% during nighttime periods.[9] A 3-D model estimates that in vast areas of the northern and southern hemisphere at least 40% of the total nitrate could be found on dust.[10]

In addition, model calculations[11−13] of the [HNO_3] to [NOx] ratio in the troposphere are consistently greater (by a factor of 5−10) than the experimentally determined value of between 1 and 9 (see, e.g., refs 11 and 14). The divergence between calculation and measurement could be reduced by including in the model an additional process that converted HNO_3 to NOx. On the other hand, the fact that several models were able to reproduce well the measured winter [HNO_3] to [NOx] ratios but not the summer ones[15] may imply the presence of a missing sink for HNO_3 that shows a strong seasonal variability. The strong seasonal variation in mineral dust concentrations, with maximum emissions in the spring and summer months and lower emissions in the winter and autumn months, means that mineral dust could make a potentially significant impact on the distribution of HNO_3 in the atmosphere and its seasonal variability.

There is also strong experimental evidence that indicates an important role for mineral dust in modifying atmospheric trace gas distributions. Mineral dust from central Asia has frequently been found to be associated with nitrate and sulfate, the concentrations of which increase with transport time over the Japanese islands.[16,17] Similar results have been reported for several northern Pacific islands,[18,19] for the western North Atlantic,[5] for the northwestern Indian Ocean,[20] for the USA,[21] and for the East Mediterranean Sea.[22]

Despite the results of field observations and modeling studies, there have been very few laboratory experiments that investigate the heterogeneous reactivity of HNO_3 on mineral aerosol. In the present work, we used a newly commissioned Knudsen reactor to investigate uptake and reaction of HNO_3 with selected authentic dust samples (Saharan dust from Cape Verde and Arizona dust) and with powder samples of $CaCO_3$ and Al_2O_3. Experiments on $CaCO_3$ were performed because calcite is a frequent constituent of desert dust (up to 30% of the total aerosol

* To whom correspondence should be addressed.

10.1021/jp001254+ CCC: $20.00
Published on Web 03/01/2001

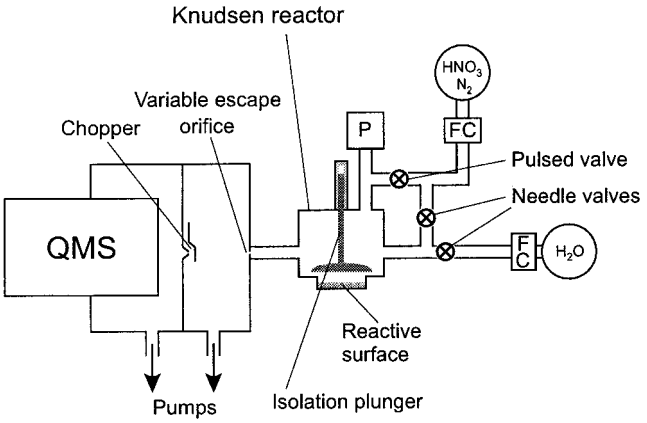

Figure 1. Schematic diagram of the experimental setup including Knudsen reactor, quadrupole mass spectrometer (QMS), and mixing line with flow controllers (FC). The pressure in the Knudsen reactor was generally 0.4 mTorr; the pressure in the mixing line held constant at 0.5 Torr. The pressure in the MS chamber was $\approx 10^{-6}$ Torr.

mass for northern Saharan dust[23]) and which, because of its alkalinity, is thought to make a considerable contribution to the uptake of acidic trace gases on mineral aerosol. Experiments on grain-size selected samples of Al_2O_3 were performed in order to characterize the experimental setup and data analysis. Saharan dust from Cape Verde is highly suited for uptake measurements because it is characteristic of the mineral aerosol that is transported from the Sahara over the Atlantic Ocean.[24]

In this study, we present uptake coefficients for HNO_3 on the above-mentioned substrates at room temperature, combined with an evaluation of the influence of water on the uptake process.

2. Experimental Section

This is the first description of the newly commissioned Knudsen reactor setup, which is therefore presented in detail. A schematic diagram is given in Figure 1.

2.1. Knudsen Reactor/Mass Spectrometer (MS). The Knudsen reactor consists of two parts. The upper part, supporting the isolation plunger, is made from Pyrex glass and is fixed to the gas mixing line; the lower part, which contains the sample, is made of stainless steel and can be heated to 450 K. Both the plunger and the lower part are coated with Teflon (DuPont FEP 121-A). The main compartment is 32 mm high and has a diameter of 70 mm; the sample compartment is 15 mm high and has a diameter of 30 mm. The total volume, including the connections to the MS and to the pressure gauge, is just 150 cm^3. The volume of the sample compartment was kept small (10.6 cm^3) in order to reduce artifacts caused by changes in the Knudsen reactor volume after the plunger is raised. The pressure inside the Knudsen reactor was measured with a pressure gauge (MKS Baratron 627, 0.01−100 mTorr). The Knudsen reactor was coupled to the MS via a variable diameter escape orifice (hole diameters in mm: 10.0, 5.9, 3.5, 2.0, 1.2, and 0.7). In the present experiments, we used the 10.0, 5.9, and 3.5 mm orifices. Before entering the MS, the molecular beam was modulated by a punched wheel chopper at 244 Hz, permitting phase-sensitive detection. The molecular beam was ionized with a cross-beam rhenium ion source. Ions were mass selected with a quadrupole mass analyzer and detected with a secondary electron multiplier. Data were accumulated by an ion-counting preamplifier and were finally stored in a PC.

The MS signal is proportional to the molecular flow through the Knudsen reactor. The parameter describing the loss of molecules through the orifice under molecular flow conditions is the escape rate constant k_{esc}. Theoretically, the escape rate constant is related to the orifice size by

$$k_{esc} = \frac{\bar{c} A_{esc}}{4V} \qquad \text{(i)}$$

where $\bar{c}$ is the average molecular velocity of the gas molecules, A_{esc} is the surface area of the escape orifice, and V is the Knudsen reactor volume. This expression corresponds to the "collision" frequency of a gas molecule with the area of the escape orifice. In practice, the experimental escape rate is smaller than the theoretical one because of flow resistance in the connection between Knudsen reactor and MS.

In the present setup, k_{esc} is determined in a pulsed valve experiment in which a short pulse of an unreactive gas is introduced into the Knudsen reactor. The decay of its concentration in the Knudsen reactor is monitored with the MS and found to be exponential:

$$C(t) = C_0 \exp(-k_{esc} t) \qquad \text{(ii)}$$

However, pulsed valve experiments with HNO_3 do not provide reliable escape rate constants because HNO_3 is a molecule with a high affinity for surfaces and loss to nonpassivated reactor walls competes with effusion through the orifice. To determine the escape rate constants for the six orifice sizes, we performed pulsed valve experiments with a number of other gases: N_2 (28 atomic mass units (amu)), Ar (40 amu), NO_2 (46 amu), SO_2 (64 amu), and $CFCl_3$ (136 amu). From the results obtained we derived a general molecular mass dependent expression for the escape rate constants. The average molecular velocity $\bar{c}$ (in units of cm/s) depends on the molar mass M of the gas molecule, as shown by eq iii:

$$\bar{c} = 1.46 \times 10^4 \sqrt{T/M} \qquad \text{(iii)}$$

where T is the absolute temperature (298 K) and M is the molar mass (in g). The appropriate temperature and mass dependent expressions for calculating k_{esc} are given in Table 1. They hold for HNO_3 (63 amu) as soon as the walls of the Knudsen reactor are passivated with HNO_3.

The flows of the reactant gases through the mixing line were controlled by actively regulating the pressure at 0.5 Torr. Gases entered the Knudsen reactor either by a second needle valve or via a pulsed valve. All needle valves were constructed of Teflon and were heated to 313 K to eliminate the influence of temperature fluctuations. The needle valves were used for continuous-flow steady-state experiments, the pulsed valve was used for experiments in which a dosed pulse of gas was introduced into the Knudsen reactor (pulse duration ~20 ms).

TABLE 1: Knudsen Reactor Parameters

Knudsen reactor parameter	value
volume, V	150 cm^3
temperature, T	298 K
total pressure, p	0.4 mTorr
HNO_3 number density	$6.5 \times 10^{10}-1.3 \times 10^{12}/cm^3$
HNO_3 flow	$2.5 \times 10^{13}-1.8 \times 10^{15}/s$
escape orifice #4 diameter	3.5 mm
escape orifice #5 diameter	5.9 mm
escape orifice #6 diameter	10.0 mm
escape orifice #4 escape rate, $k_{esc,4}$	0.309 $(T/M)^{1/2}$ s^{-1}
escape orifice #5 escape rate, $k_{esc,5}$	1.098 $(T/M)^{1/2}$ s^{-1}
escape orifice #6 escape rate, $k_{esc,6}$	4.235 $(T/M)^{1/2}$ s^{-1}
sample surface area, A_s	1.5 and 4.8 cm^2
sample collision frequency, ω	81.31 and 255.24 s^{-1}

2.2. Reactant Gas Preparation. HNO_3 was prepared by dissolving 80 g of KNO_3 (Aldrich) in 150 mL of concentrated H_2SO_4 (95−97%; Aldrich) at 273 K. The HNO_3 vapor was transferred to a trap at liquid nitrogen temperature and finally stored as anhydrous HNO_3 liquid in a blackened bulb at 233 K. Gas-phase samples of HNO_3 with N_2 (mixing ratios of 0.1, 0.04, and 0.005) were prepared using standard manometric techniques and stored in 2 L blackened glass vessels. Optical absorption measurements performed on these samples revealed the presence of NO_2 impurity at <2% level. DNO_3 was prepared using D_2SO_4 (98% in D_2O; Aldrich) instead of H_2SO_4.

2.3. Dust Sample Characterization and Preparation. Al_2O_3 (α-Al_2O_3) and $CaCO_3$ were purchased from Sigma-Aldrich. For Al_2O_3, we chose four disjunctive size classes ($d < 10$ μm, 10 μm $< d <$ 44 μm, 44 μm $< d <$ 74 μm, and 74 μm $< d <$ 149 μm). $CaCO_3$, ATD ("Arizona test dust"; Powder Technology, Inc., MN, USA), and SDCV (Saharan dust from Cape Verde islands, provided by L. Gomes) particles were smaller than 10 μm. In addition, we carried out some experiments on polished and unpolished $CaCO_3$ (104) and α-Al_2O_3 ($11\bar{2}0$) single crystals (purchased from MaTecK, Jülich, Germany).

The mineral dust samples were prepared by mixing 30, 60, or 100 mg of dust into a paste with water or ethanol and dispersing on a round optical glass flat (surface area $A_s = 1.5$ or 4.8 cm^2), which was then placed in the sample compartment. Experiments using H_2O for dispersing the mineral dust gave the same results as the ones using ethanol. Ethanol was used for the majority of the experiments because it dries much faster. The bulk density of the sample was determined from its weight and height, which was measured using calibrated feeler gauges.

The $CaCO_3$ and Al_2O_3 single crystals had a size of 10 × 10 × 0.5 and 10 × 10 × 1 mm^3, respectively. Dust samples and single crystals were usually heated to 363 K for 5 h under vacuum ($p \approx 2 \times 10^{-6}$ Torr) and held under vacuum overnight in the Knudsen reactor prior to the experiment. BET surface areas of the mineral dust were determined with a Quantachrome Autosorb 6B. Scanning electron microscopy of unsputtered surfaces was carried out with a LEO Gemini 1530 operated at 1.5 kV.

2.4. Measurement Procedure and Data Analysis. Uptake coefficients, γ, were determined in steady-state, continuous-flow experiments at room temperature (298 K). To make sure that molecule−surface interactions dominate over molecule−molecule interactions, Knudsen experiments must be carried out in the Knudsen pressure regime or in the molecular flow regime. The Knudsen regime requires the mean free path to be similar to the dimensions of the reactor; at lower pressures, molecular flow dominates. In the present experiments, a total Knudsen reactor pressure of $p = 0.4$ mTorr was used, which is in the molecular flow regime. The HNO_3 concentration was determined from the HNO_3 mixing ratio, which was checked with UV spectroscopy, and the Knudsen reactor pressure. The HNO_3 concentration was varied between 1.3×10^{12}, 5.2×10^{11}, and 6.5×10^{10} cm^{-3}. The corresponding HNO_3 flows through the Knudsen reactor into the MS were between 1.8×10^{15} and 2.5×10^{13} s^{-1} depending on the size of the escape orifice.

The uptake probability γ is defined as the ratio of the number of collisions with the surface that lead to removal from the gas phase to the total number of collisions with the surface. This is mathematically equivalent to

$$\gamma = \frac{k_{uni}}{\omega} \qquad \text{(iv)}$$

where ω is the collision frequency of a molecule with the reactive surface area of the sample A_s (see Table 1) and is calculated from

$$\omega = \frac{\bar{c}A_s}{4V} \qquad \text{(v)}$$

The unimolecular rate constant k_{uni} is defined for a pseudo-first-order removal of the reactant gas from the gas phase to the reactive surface, which depends on the number of available surface sites for the heterogeneous interaction. k_{uni} is obtained by measuring the relative height of the signal before and during exposure to the dust surface:

$$k_{uni} = \left(\frac{S_0}{S(t)} - 1\right)k_{esc} \qquad \text{(vi)}$$

where S_0 is the MS signal of the reactant gas prior to the lifting of the plunger and $S(t)$ is the time dependent signal over the whole duration of the experiment. Note that $S(t)$ is corrected for the small uptake of HNO_3 observed when no dust was present in the sample compartment of the Knudsen reactor (see Figure 2).

The uptake coefficient is thus given by

$$\gamma = \frac{k_{esc}}{\omega}\left(\frac{S_0}{S(t)} - 1\right) \qquad \text{(vii)}$$

For the determination of γ, HNO_3 was monitored at its strongest fragment at m/e 46 (NO_2^+). The integration time for the signal

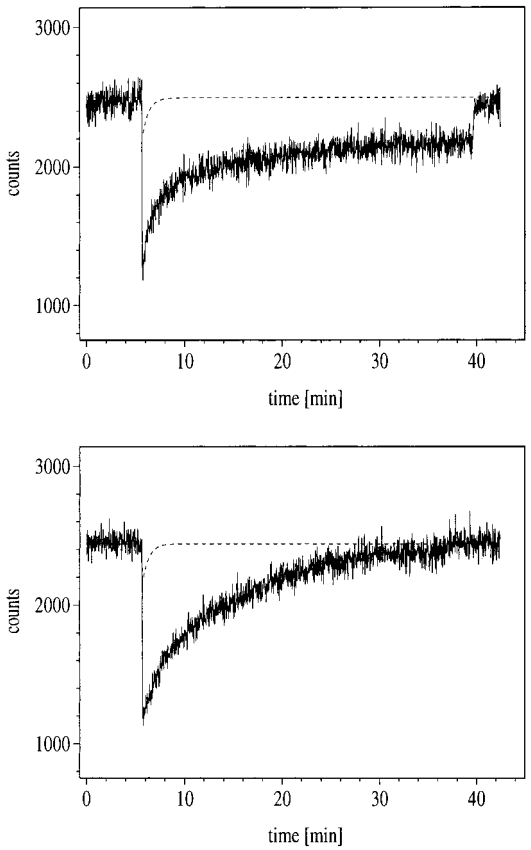

Figure 2. The uptake of HNO_3 onto ≈60 mg of Al_2O_3. Upper panel: small grain size ($d < 10$ μm). Lower panel: large grain size (44 μm $< d <$ 74 μm). The dashed lines indicate the size and shape of HNO_3 uptake in the absence of a dust sample, which has already been subtracted for the experimental trace. Details of the experimental conditions are found in Table 2, experiments A23 and A25, respectively.

was 0.8 s with a duty cycle of 1.7 s. In some experiments, HNO_3 was also monitored at *m*/*e* 30 (NO^+) and *m*/*e* 63 (HNO_3^+) in order to make sure that the *m*/*e* 46 signal was representative of the HNO_3 concentration and that there were no contributions from NO_2. The ratios *m*/*e* 63 to *m*/*e* 46 and *m*/*e* 63 to *m*/*e* 30 remained constant during the exposure, showing that HNO_3 does not decompose to NO_2 on the reactor walls or react with the dust sample to form significant amounts of gaseous NO, NO_2, or HONO. In the experiments on $CaCO_3$, H_2O was monitored on *m*/*e* 17 (OH^+) or *m*/*e* 18 (H_2O^+) and CO_2 on *m*/*e* 44 (CO_2^+).

2.5. Error Analysis. Three quantities in eq vii contributed to the experimental error of γ: k_{esc}, ω, and *S*. k_{esc} was determined with an accuracy of 4.3% for the 10 mm escape orifice and 4.5% for the 5.9 mm escape orifice (4.4% on average). The error of ω was mainly determined by the uncertainty in the Knudsen reactor volume which was estimated to be 6.7%. The sample surface area A_s, corresponding to the surface area of the glass flat covered with dust or to the surface area of the single crystal, did not significantly contribute to the error of ω because it could be measured very precisely. Finally, the uncertainty of the MS signal (*S*) after opening the plunger was determined by the random noise and came to maximal 2.5% for the low flow experiments. The three errors add up to a total error of 8.4% for the resulting γ. However, in some cases, the reproducibility of the measured uptake coefficient was considerably worse than this, indicating that systematic errors, probably related to surface preparation and presentation, are the dominant source of error. We therefore quote an error of $\pm$ 25%, based on the maximum observed fluctuations from the mean value of γ that were observed in the course of these studies. Later we consider potential errors associated with the usage of the geometric surface area to calculate the uptake coefficient rather than a surface area that takes into account the internal surface of the sample.

3. Results and Discussion

The results are presented in separate sections according to the substrate used. For each substrate, sample mass, geometric surface area, and HNO_3 flow were varied. For Al_2O_3, the grain size was also systematically varied. In addition, experiments were conducted using Al_2O_3 and $CaCO_3$ single crystals. In all cases, the initial rate of uptake of HNO_3 onto the dust surface was determined, which is taken as a measure of the reactivity of fresh mineral dust surfaces. The role of adsorbed water on the uptake process and on the formation of reaction products was also examined.

3.1. Uptake of HNO_3 onto Al_2O_3. In total, 26 experiments were carried out using Al_2O_3 samples with different grain sizes: $d < 10$ μm, 10 μm $< d <$ 44 μm, 44 μm $< d <$ 74 μm, and 74 μm $< d <$ 149 μm. The results are presented in Table 2, along with the experimental conditions in each case.

Typical raw data from an experiment to investigate the uptake of HNO_3 onto $\approx$ 60 mg of Al_2O_3 are shown in Figure 2. After a steady flow of HNO_3 has been established, the isolation plunger is lifted (at $t = 6$ min) and the surface is exposed to the HNO_3 flow. Because of uptake of HNO_3 onto the Al_2O_3, the number of molecules exiting through the escape orifice into the MS decreases immediately. As the exposure time increases, the HNO_3 signal recovers, indicating a decrease in the number of available sites for reaction, resulting in an apparent reduction in the uptake coefficient. At $t = 40$ and 37 min respectively, the plunger is lowered and the HNO_3 signal returns to its initial steady-state value.

Comparison of the uptake profiles in Figure 2 reveals differences in the uptake process. The HNO_3 uptake onto Al_2O_3 with $d < 10$ μm (upper panel) takes place in two phases: In the first four minutes of exposure (6 min $< t <$ 10 min), the HNO_3 signal quickly recovers to $\approx$75% of its original value, whereas at $t > \sim$10 min, the recovery is much slower. In the case of HNO_3 onto larger grain-sized Al_2O_3 (44 μm $< d <$ 74 μm, lower panel), the recovery of the MS signal proceeds continuously and has almost reached the steady-state level after 37 min of exposure. These differences can be understood in terms of external surface saturation and diffusion into the bulk. We examined this aspect of the uptake process in more detail by taking electron micrographs of both Al_2O_3 ($d < 10$ μm) and Al_2O_3 (44 μm $< d <$ 74 μm) samples that had been prepared in an identical manner to those used in the Knudsen reactor experiments. These micrographs are displayed in Figure 3a ($d < 10$ μm) and Figure 3b (44 μm $< d <$ 74 μm). They show the different surface morphologies of the two grain sizes. In addition, we carried out BET surface area measurements of each dust sample. The measured Al_2O_3 BET surface areas are: ($d <$ 10 μm) = 1.5 m^2/g, (10 μm $< d <$ 44 μm) = 0.5 m^2/g, (44 μm $< d <$ 74 μm) = 0.3 m^2/g, and (74 μm $< d <$ 149 μm) = 0.1 m^2/g. Clearly, and as expected, the total surface area is significantly larger for the smaller particles (by a factor of $\approx$15), explaining the larger capacity for this sample to remove HNO_3 from the gas phase, as evidenced by the slower signal recovery. The difference in the time dependence of the HNO_3 uptake onto different grain sizes of Al_2O_3, as exemplified in Figure 2, is related to the difference in the total available surface area and to differences in the rate of diffusion into the internal voids of the dust sample. This is expected to take place on a longer time scale than uptake on external surface sites and is faster for the larger grain size.

From our experiments, it is not possible to draw quantitative conclusions concerning the capacity of mineral dust to react

TABLE 2: Summary of Uptake Experiments with HNO_3 onto Al_2O_3

expt	grain[a]	geometric surface area (cm^2)	sample mass (mg)	Ø escape orifice (mm)	$[HNO_3]$ (cm^{-3})	γ_{init} $\times 10^{-2}$
A1	1	4.8	100	5.9	1.3×10^{12}	4.4
A2	2	4.8	100	5.9	1.3×10^{12}	2.9
A3	3	4.8	110	5.9	1.3×10^{12}	4.0
A4	4	4.8	120	5.9	1.3×10^{12}	4.1
A5	1	1.5	100	5.9	1.3×10^{12}	5.5
A6	1	1.5	100	5.9	5.2×10^{11}	4.6
A7	2	1.5	100	5.9	5.2×10^{11}	2.9
A8	3	1.5	100	5.9	5.2×10^{11}	5.3
A9	4	1.5	100	5.9	5.2×10^{11}	4.4
A10	1	1.5	60	5.9	5.2×10^{11}	5.3
A11	2	1.5	60	5.9	5.2×10^{11}	3.1
A12	3	1.5	60	5.9	5.2×10^{11}	4.1
A13	4	1.5	60	5.9	5.2×10^{11}	4.1
A14	1	1.5	100	5.9	6.5×10^{10}	9.7
A15	1	1.5	60	10	1.3×10^{12}	6.5
A16	2	1.5	60	10	1.3×10^{12}	5.9
A17	3	1.5	60	10	1.3×10^{12}	7.1
A18	4	1.5	60	10	1.3×10^{12}	5.7
A19	1	1.5	60	10	5.2×10^{11}	11.9
A20	4	1.5	100	10	5.2×10^{11}	10.2
A21	4	1.5	60	10	5.2×10^{11}	11.8
A22	4	1.5	30	10	5.2×10^{11}	10.4
A23	1	1.5	60	10	6.5×10^{10}	12.6
A24	2	1.5	60	10	6.5×10^{10}	8.2
A25	3	1.5	60	10	6.5×10^{10}	13.2
A26	4	1.5	60	10	6.5×10^{10}	13.4

[a] Grain 1, ($d < 10$ μm), BET surface area = 1.5 m^2/g; Grain 2, (10 μm $< d <$ 44 μm), BET surface area = 0.5 m^2/g; Grain 3, (44 μm $< d <$ 74 μm), BET surface area = 0.3 m^2/g; Grain 4, (74 μm $< d <$ 149 μm), BET surface area = 0.1 m^2/g.

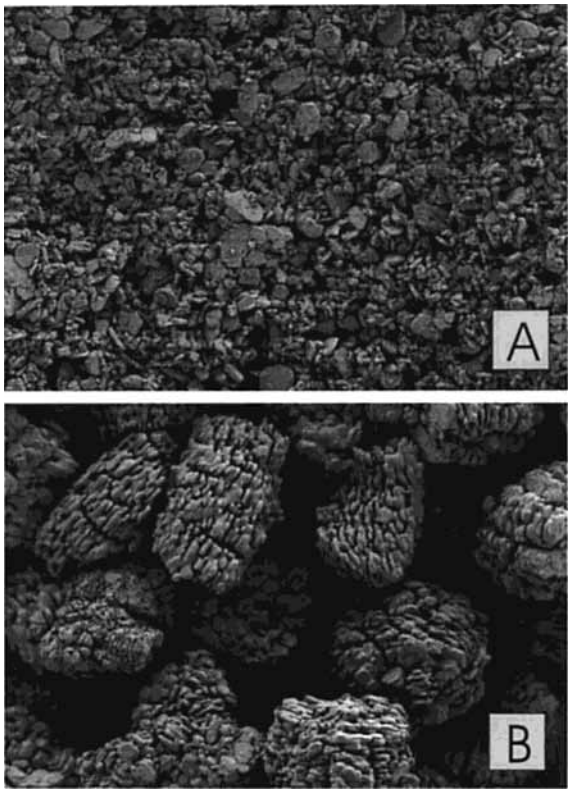

Figure 3. Electron micrographs of the Al_2O_3 samples prepared as usual for the Knudsen reactor experiments. (A) grain size $d < 10$ μm and (B) grain size 44 μm $< d <$ 74 μm. In both figures, the full width of the micrograph is 270 μm.

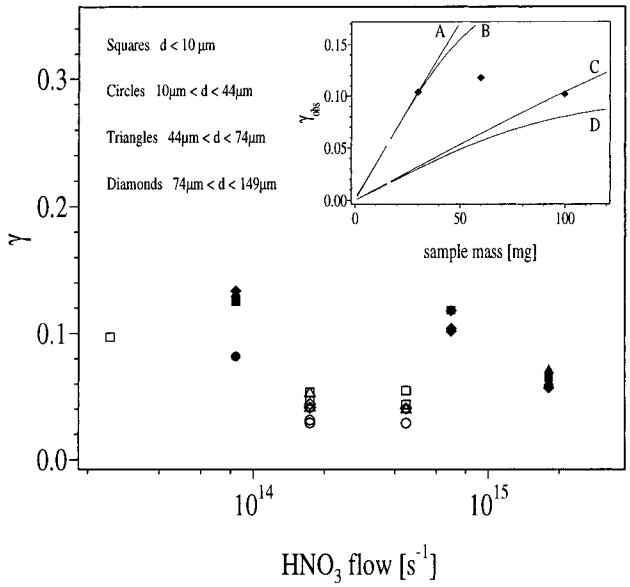

Figure 4. Uptake of HNO_3 onto Al_2O_3: dependence of the uptake coefficients on the flow of HNO_3. The open symbols represent data obtained with the 5.9 mm escape orifice; the filled symbols represent data obtained with the 10 mm escape orifice. Insert: initial uptake coefficient (γ_{obs}) vs sample mass (expts A20−A22). The initial HNO_3 concentration was held constant at 5.2×10^{11} cm^{-3}; the Al_2O_3 sample was the 74−149 μm grain size. The solid curves were calculated according to the pore diffusion model as described in the text with $\bar{d}$ = 112 μm, A^{BET} = 0.1 m^2/g, ρ_t = 3.97 g/cm^3, and ρ_b = 1.8 g/cm^3. Curve A, $\tau = 2$, $\gamma^{pd} = 5.5 \times 10^{-3}$; Curve B, $\tau = 20$, $\gamma^{pd} = 5.5 \times 10^{-3}$; Curve C, $\tau = 2$, $\gamma^{pd} = 2.4 \times 10^{-3}$; and Curve D, $\tau = 20$, $\gamma^{pd} = 2.4 \times 10^{-3}$.

with HNO_3 under atmospheric conditions. The use of bulk samples in the experiments means that the dust presentation and interaction with the gas phase is different from that which takes place in the atmosphere. However, one parameter of the heterogeneous uptake can accurately be determined: the initial uptake probability, i.e., the uptake probability immediately after the lifting of the plunger. Therefore, the further discussion of our results focuses on this parameter:

$$\gamma_{init} = \frac{k_{esc}}{\omega}\left(\frac{S_0}{S(t_{open})} - 1\right) \qquad \text{(viii)}$$

where t_{open} is the time at which the sample was first exposed by lifting the isolation plunger. Because the major goal of the experiments using Al_2O_3 was to establish the experimental procedure and to identify the correct surface area for calculating the uptake coefficient, a series of diagnostic experiments were carried out in which important experimental parameters such as the sample mass and the geometric surface area were varied.

In six sets of experiments (Expts A1−A4, A6−A9, A10−A13, A15−A18, A19 and A21, and A23−A26; Table 2) we examined in detail the influence of the substrate's grain size on the initial HNO_3 uptake, with the mass of substrate held constant. γ_{init} was found to vary within the limits of uncertainty if the results for one middle range grain size, 10 μm $< d <$ 44 μm, are excluded. We assume that this batch was somehow contaminated.

The invariability of γ_{init} with grain size has an important consequence. First, the BET surface, which varies over 1 order of magnitude (see footnotes to Table 2) is not the appropriate reactive surface area for the calculation of γ. If diffusion of HNO_3 into the internal pores of the dust sample contributed significantly to the initial uptake, we should have seen an increase in k_{uni} with decreasing grain size because of the increasing internal surface area. k_{uni}, however, was completely unaffected by the variation of grain size. This important aspect of the uptake is discussed in detail in section 3.6. The use of different geometric surface areas (i.e., 4.8 cm^2 rather than the standard 1.5 cm^2, experiments A1−A4) yielded values for γ_{init} which are in the same range as the values of the experiments A6−A13. Experiments A1−A4 were performed at a higher HNO_3 flow than experiments A6−A13, but experiment A5 shows that in this regime within the limits of uncertainty the flow has no influence on the initial uptake (compare to A8).

A double series of experiments (A6−A13) was performed with 60 and 100 mg and a third series (A20−A22) with 30, 60, and 100 mg of Al_2O_3 spread on 1.5 cm^2 glass flats. γ_{init} did not show any dependency on the sample mass, i.e., γ_{init} did not depend on the thickness of the bulk sample. Only the uptake capacity of the Al_2O_3 bulk increases with increasing sample mass.

In Figure 4, we plot the initial uptake coefficient vs the flow of HNO_3. The HNO_3 flow was varied by using different mixing ratios in N_2 in the storage bulb and different escape orifices. Values of γ obtained in experiments with the 5.9 mm escape orifice are lower than the ones obtained with the 10 mm escape orifice, and both sets show an increase in γ with decreasing HNO_3 flow. This can be explained by Knudsen reactor wall effects. After a steady concentration of HNO_3 has been established, HNO_3 adsorbed on the walls is in equilibrium with the gaseous HNO_3 in the Knudsen reactor. As soon as the plunger is lifted this equilibrium is perturbed because of fast uptake of HNO_3 onto the dust surface, and the reactor walls act as an additional HNO_3 source. That HNO_3 is lost, indeed, from the reactor walls can clearly be seen after lowering the plunger, after which the HNO_3 signal takes up to two minutes

TABLE 3: Summary of Uptake Experiments with HNO_3 onto $CaCO_3$

expt	geometric surface area (cm^2)	sample mass (mg)	sample condition	Ø escape orifice (mm)	$[HNO_3]$ (cm^{-3})	$\gamma_{init} \times 10^{-2}$
B1	4.8	100	unreacted, dry	5.9	1.3×10^{12}	5.0
B2	4.8	100	reacted, dry	5.9	1.3×10^{12}	0.9
B3	4.8	100	reacted, dry	5.9	1.3×10^{12}	1.6
B4	1.5	100	unreacted, dry	5.9	1.3×10^{12}	5.1
B5	1.5	100	reacted, dry	5.9	1.3×10^{12}	2.1
B6	1.5	100	unreacted, dry	5.9	5.2×10^{11}	5.2
B7	1.5	100	unreacted, damp	5.9	6.5×10^{10}	9.9
B8	1.5	60	unreacted, damp	10	1.3×10^{12}	7.3
B9	1.5	60	reacted, damp	10	1.3×10^{12}	7.3
B10	1.5	60	unreacted, damp	10	5.2×10^{11}	13.7
B11	3.1	100	unreacted, dry	10	5.2×10^{11}	4.3
B12	3.1	100	unreacted, dry	10	5.2×10^{11}	6.9
B13	3.1	100	unreacted, dry	10	5.2×10^{11}	6.3
B14	3.1	100	reacted, dry	10	5.2×10^{11}	2.8
B15	4.8	100	unreacted, dry	10	5.2×10^{11}	7.0
B16	1.5	60	unreacted, damp	10	1.0×10^{11}	18.3
B17	1.5	60	reacted, damp	10	6.5×10^{10}	16.2
B18	1.5	60	reacted, damp	10	6.5×10^{10}	15.1
B19	1.5	60	unreacted, dry	10	6.5×10^{10}	9.3
B20	1.5	60	unreacted, dry	10	6.5×10^{10}	11.6
B21	1.5	60	unreacted, dry	10	6.5×10^{10}	10.2
B22	1.5	60	unreacted, dry	10	6.5×10^{10}	7.8

to increase to its original steady-state value, showing that the walls have been depassivated and again act as a sink for HNO_3. Degassing of HNO_3 from the walls during the uptake process distorts the results because the MS signal is enhanced with respect to the ideal case without degassing. This effect means that measured uptake coefficients are lower than the actual ones and become more important with larger k_{uni} because the difference between S_0 and $S(t_{open})$ is larger. It also explains why uptake coefficients measured with the 5.9 mm escape orifice are smaller than the ones measured with the 10 mm escape orifice, because the drop in signal for the small escape orifice is larger because of a longer residence time in the reactor. For this reason, uptake coefficients measured with the 10 mm escape orifice at small HNO_3 flows are closest to the real value because k_{uni} is minimized. The preferred uptake coefficient for HNO_3 onto Al_2O_3 is thus an average of the results from experiments A23, A25, and A26 and is $(13 \pm 3.3) \times 10^{-2}$.

3.2. Uptake of HNO_3 onto $CaCO_3$. A total of 22 experiments with $CaCO_3$ powder samples were carried out, and the results are presented in Table 3 and in Figures 5 and 6. For the $CaCO_3$ experiments, we observed a strong influence of surface water, both in the uptake coefficients and in the formation of gas-phase products. Here we adopt the arbitrary definition of "damp" as applying to dust that has not been heated before the uptake of HNO_3 was measured and "dry" for dust samples that had been heated in the standard manner to 363 K and kept in the evacuated Knudsen reactor overnight.

3.2.1. Uptake Coefficient. The raw data from an experiment to investigate the uptake of HNO_3 onto $CaCO_3$ is shown in Figure 5. The presence of water on the $CaCO_3$ sample is indicated by the peak at *m*/*e* 17 immediately after lifting the plunger at $t = 6$ min. This short-lived signal originates from surface-adsorbed water that had already been released from the sample to the gas phase and trapped in the isolated volume under the plunger. This water signal is missing in experiments where the sample was heated. Initial uptake coefficients on fresh $CaCO_3$ samples were in the range of 0.05−0.18 and, within experimental uncertainty, were independent of the geometric surface area (expt B1 vs B4).

Uptake coefficients as a function of flow are plotted in Figure 6. Two series of experiments (B11−B13 and B19−B22) can

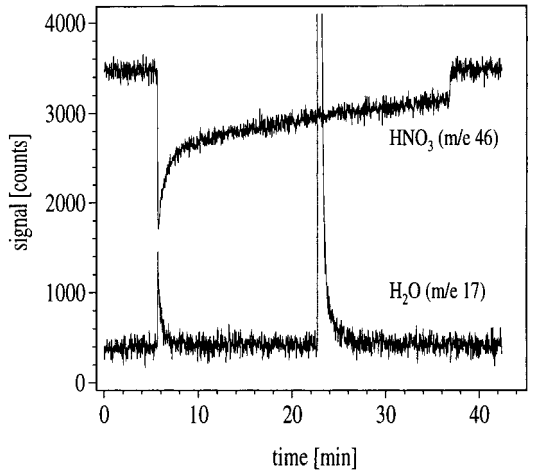

Figure 5. Uptake of HNO_3 onto $CaCO_3$: raw data (expt B16). Upon lifting the plunger at $t \approx 6$ min, some H_2O is released from the dust sample. After ≈17 min exposure, an extra flow ($\approx 2.3 \times 10^{16}$ s^{-1}) of H_2O was added to the reactor (*m*/*e* 17). The HNO_3 signal at *m*/*e* 46 has been shifted up by 1000 counts for clarity.

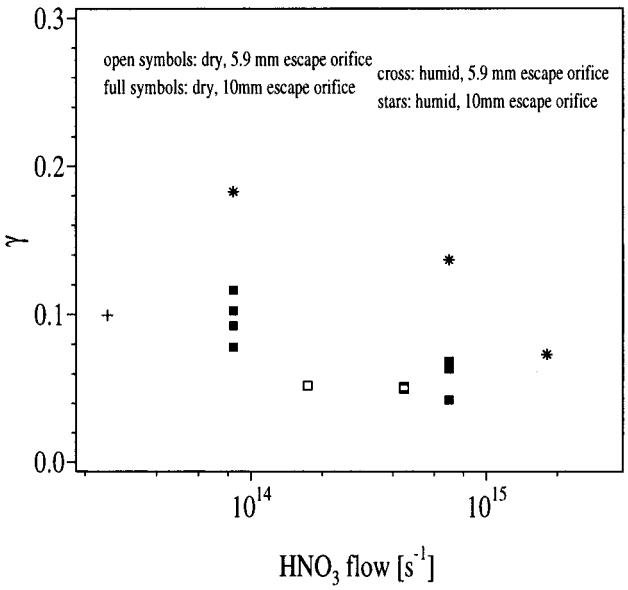

Figure 6. Uptake of HNO_3 onto $CaCO_3$: dependence of the uptake coefficients on the flow of HNO_3. The open symbols represent data obtained with the 5.9 mm escape orifice; the filled symbols represent data obtained with the 10 mm escape orifice.

be taken as a test of the reproducibility of the uptake measurement: the values show reasonable agreement, though not within the expected experimental error. Comparison of these γ_{init} values to the γ_{init} values from experiments B10 and B16, respectively, shows that under certain conditions the uptake coefficient can be two or three times higher. The difference in the results can be explained by the presence of water, because both the initial uptake coefficient and the rate of surface saturation are highly dependent on the water content of the $CaCO_3$ sample, with a higher uptake on damp $CaCO_3$ (e.g., B16) and a smaller uptake on dry $CaCO_3$ (e.g., B19−B22).

For experiments on dry as well as on damp $CaCO_3$ samples, a decrease in the uptake coefficient with increasing flow and decreasing escape orifice size was observed. In Figure 6, the stars and the cross are results from experiments on damp $CaCO_3$ and the squares are from experiments on dry $CaCO_3$. It is interesting to note that the impact of high HNO_3 flows is bigger for experiments on damp substrates because they have higher uptake probabilities. In a single experiment, we investigated the

effect of adding water during the uptake process in order to see if a chemically aged surface (after exposure to HNO_3) can thereby be reactivated. The addition of a flow of H_2O (2.3×10^{16} s^{-1}) at $t \approx 22.5$ min has no influence on the rate of decline of the HNO_3 uptake coefficient (Figure 5), suggesting that this is not the case, at least on the time scales and the H_2O concentrations available in this experimental setup. The final result for dry $CaCO_3$ is $\gamma = (9.7 \pm 2.4) \times 10^{-2}$, which is the value we determined at low HNO_3 concentrations.

Several experiments were also performed on prereacted $CaCO_3$. After saturation of the sample with HNO_3 (i.e., the sample was exposed to HNO_3 until the uptake coefficient had decreased to almost zero), the HNO_3 flow was shut off and the sample was left in the Knudsen reactor, which was evacuated overnight. A total of 24 h after the first exposure, the experiment was repeated. We found that the initial reactivity is partly or almost fully restored, depending on sample heating. Experiments B9 and B17−B18 were performed on damp $CaCO_3$ that already had reacted with HNO_3 the day before. Uptake coefficients almost reached the value of the unreacted sample. However, the time required for the uptake to reach saturation is strongly reduced, indicating a decrease in bulk reactivity. Apparently, external surface sites that had been saturated are again available for reaction after 24 h. At the same time, the number of reactive sites inside the bulk of the sample has decreased. Experiments B2−B3, B5, and B14 were performed on dry $CaCO_3$. Uptake coefficients of HNO_3 on prereacted dry $CaCO_3$ were ca. one-third of the original value. An exception is experiment B2 which was carried out only 1 h after experiment B1 and where the initial uptake coefficient is even lower. In addition, all experiments on dry, prereacted $CaCO_3$ showed that less HNO_3 was needed to deactivate the sample than in experiments on damp, prereacted $CaCO_3$.

We interpret our results in terms of surface reactivation by nitrate recrystallization. Several studies have defined the important role of surface adsorbed water in the reaction of HNO_3 with NaCl surfaces, where a water mediated recrystallization process is responsible for regeneration of reactive surface sites.[25−28] We transfer this model to $CaCO_3$, although $CaCO_3$ is hydrophobic, because water is probably bound primarily to surface defects such as edges and steps, and we extend the model also to the internal surface. Our results with single crystals (see later) suggest that the relatively smooth crystal surfaces themselves do not significantly contribute to the uptake process.

3.2.2. Product Formation. HNO_3 is expected to react with $CaCO_3$ according to

$$2HNO_3(g) + CaCO_3(s) \rightarrow Ca(NO_3)_2(s) + CO_2(g) + H_2O(g) \quad (1)$$

The formation of gas-phase products in the reaction of HNO_3 with $CaCO_3$ was investigated in experiments performed at high HNO_3 flows (1.8×10^{15} s^{-1}) and with maximal $CaCO_3$ sample surface area (4.8 cm^2). Under these conditions, both CO_2 and H_2O could be observed by mass spectrometry.

To better differentiate between water produced in the reaction of nitric acid with $CaCO_3$ and water present in the backgound, we performed an additional series of experiments with DNO_3 instead of HNO_3. A typical experiment is shown in Figure 7. DNO_3 was monitored on *m*/*e* 64 (not shown) and *m*/*e* 46, and D_2O, on *m*/*e* 20. As expected, the reaction led to the formation of D_2O, though HDO was also detected at a similar concentration. D_2O (and HDO) production was as variable as H_2O production in the reaction of HNO_3 with $CaCO_3$. Comparison

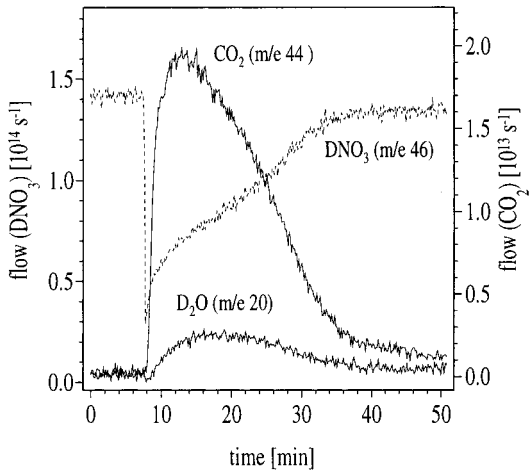

Figure 7. Uptake of DNO_3 onto $CaCO_3$. The MS signals of DNO_3 and CO_2 were put on an absolute basis by comparison with calibrated flows of each gas.

of the *m*/*e* 44 curve with the *m*/*e* 20 curve in Figure 7 shows that CO_2 production peaks at about 13 min, whereas D_2O (HDO) production peaks at about 16 min. Experiments with HNO_3 displayed a similar behavior with regard to the delayed formation of H_2O and CO_2. The delayed formation of the products is an interesting feature of HNO_3 uptake onto $CaCO_3$. We note that the delayed detection of CO_2 and H_2O cannot be due to differences in molecular flow characteristics compared to HNO_3, because both H_2O and CO_2 have smaller molecular masses and therefore larger values for k_{esc}.

In a series of experiments, we were able to show that the induction period is dependent on the HNO_3 flow, with a shorter induction period at higher HNO_3 flows. This observation is in qualitative agreement with results by Fenter et al.,[29] who observed a delayed production of CO_2 and H_2O in the reaction of HNO_3 with $CaCO_3$ and also of HCl in the reaction of HNO_3 with NaCl and KCl.[30] The present experiments revealed that the yields of CO_2 and H_2O were highly variable and depended not only on the HNO_3 flow but also on the water content of the $CaCO_3$ sample. The stoichiometry of reaction 1 was generally not fulfilled, indicating that reaction 1 does not properly describe the more complex processes occurring on the dust sample.

By calibrating the MS for CO_2 and H_2O and integrating the signals over the whole reaction time, we could show that on average 2.7 HNO_3 molecules were adsorbed for every CO_2 molecule released for "damp" dust sample. For "dry" samples, 3.4 HNO_3 molecules were consumed per CO_2 molecule released. Fenter et al.[29] also observed a reduced yield of CO_2 in the reaction of HNO_3 on dried $CaCO_3$ pellets, but they also showed that CO_2 could be released from the prereacted surface by adding a flow of water. They hypothesized that either physisorbed HNO_3 remained inactive in the absence of water or that HNO_3 formed an intermediate product with $CaCO_3$ and that CO_2 release was inhibited in the absence of surface water.

The ratio of H_2O produced to HNO_3 taken up was lower than predicted by reaction 1 by about a factor of 4 or more. Our observations for H_2O are in qualitative agreement with findings of Fenter et al.,[29] who attribute the missing water to its interaction with the $CaCO_3$ substrate. In separate experiments, in which the uptake of water on $CaCO_3$ was investigated, we were able to show that, after stopping the H_2O flow, as much H_2O degassed from the sample as had been adsorbed previously, i.e., the uptake process is reversible. These results suggest that it is not $CaCO_3$ that retains the water but the $Ca(NO_3)_2$ formed in reaction 1, which is much more hydroscopic than $CaCO_3$.

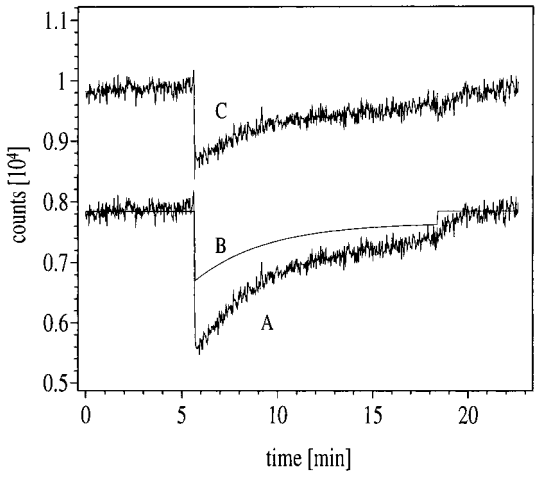

Figure 8. Uptake of HNO_3 onto an unpolished $CaCO_3$ single crystal. A, raw data; B, correction curve for uptake to the sample chamber; C, corrected data, offset by 2000 counts for clarity.

We also attempted to gain insight into the reaction mechanism by taking electron micrographs of the $CaCO_3$ sample both before and after exposure to HNO_3. No change in surface morphology was observed, and the definition of the crystal edges of the $CaCO_3$ sample was not measurably modified by treatment with HNO_3. Similar results were obtained for the Al_2O_3, ATD, and SDCV samples, and we conclude that the amounts of HNO_3 sufficient for saturation in our experiments were too low to significantly alter the surface morphology.

3.3. Single Crystals of Al_2O_3 and $CaCO_3$. In comparison with dust sample surfaces, surfaces of single crystals have very few or no defect sites. We conducted three experiments each on polished and unpolished Al_2O_3 and $CaCO_3$ single crystals, using the 3.5 mm escape orifice and an HNO_3 flow of 2.6×10^{13} s^{-1}. For Al_2O_3, we determined $\gamma = (1.6 \pm 1.4) \times 10^{-3}$ on unpolished surfaces and $\gamma = (6.7 \pm 1.9) \times 10^{-4}$ on polished surfaces. For $CaCO_3$, we determined $\gamma = (1.75 \pm 0.39) \times 10^{-3}$ on unpolished surfaces (Figure 8) and $\gamma = (9.6 \pm 1.2) \times 10^{-4}$ on polished surfaces, where the quoted errors have been chosen to reflect the reproducibility based on the total of three experiments. Uptake coefficients on single crystals are smaller than uptake coefficients on dust samples by about 2 orders of magnitude. In addition, uptake coefficients are smaller on polished surfaces than on unpolished surfaces, and the correction to $S(t)$ for uptake of HNO_3 to the walls of the sample compartment was of a similar size as the uptake of HNO_3 onto the single-crystal surface (Figure 8). Both results underline the importance of defect sites for the reactivity of the sample. It is not clear whether the uptake is reduced because there are less defect sites for direct HNO_3 uptake, or because there is less water bound to defect sites. Bearing in mind the effects described in the previous section we believe that the absence of water is the reason for the reduced uptake.

3.4. Uptake of HNO_3 onto Arizona Dust. A total of 8 experiments with ATD were carried out, and the results are listed in Table 4. Uptake coefficients were in the range between 2×10^{-2} and 7×10^{-2} and found to be independent of the geometric surface area of the sample and of the HNO_3 flow. A slight tendency of increasing uptake coefficients with decreasing HNO_3 flows was observed, with slightly higher γ values for experiments with the bigger escape orifice. The final result is $\gamma = (5.7 \pm 1.5) \times 10^{-2}$, which is the mean uptake coefficient for low HNO_3 concentrations.

3.5. Uptake of HNO_3 onto Saharan Dust. A total of 11 experiments with SDCV were carried out, and the results are listed in Table 5. Uptake coefficients were found to be independent of the geometric surface area of the sample and lie between 6×10^{-2} and 12×10^{-2}. A slight dependence of the uptake coefficient on the HNO_3 flow was found, and a value of $\gamma = (11 \pm 3) \times 10^{-2}$, the uptake coefficient for low HNO_3 concentrations, is the preferred result.

TABLE 4: Summary of Uptake Experiments with HNO_3 onto ATD

expt	geometric surface area (cm^2)	sample mass (mg)	Ø escape orifice (mm)	$[HNO_3]$ (cm^{-3})	$\gamma_{init} \times 10^{-2}$
C1	4.8	100	5.9	1.3×10^{12}	2.1
C2	1.5	100	5.9	1.3×10^{12}	2.8
C3	1.5	100	5.9	5.6×10^{11}	3.4
C4	1.5	100	5.9	6.5×10^{10}	5.0
C5	1.5	60	10	1.3×10^{12}	4.0
C6	1.5	60	10	5.6×10^{11}	6.6
C7	1.5	60	10	6.5×10^{10}	6.8
C8	1.5	60	10	6.5×10^{10}	4.7

TABLE 5: Summary of Uptake Experiments with HNO_3 onto SDCV

expt	geometric surface area (cm^2)	sample mass (mg)	Ø escape orifice (mm)	$[HNO_3]$ (cm^{-3})	$\gamma_{init} \times 10^{-2}$
D1	4.8	100	5.9	1.3×10^{12}	6.1
D2	1.5	100	5.9	1.3×10^{12}	7.2
D3	1.5	100	5.9	5.6×10^{11}	7.1
D4	1.5	100	5.9	5.6×10^{11}	11.7
D5	1.5	100	5.9	6.5×10^{10}	9.2
D6	1.5	60	10	1.3×10^{12}	10.6
D7	1.5	60	10	5.6×10^{11}	12.4
D8	1.5	60	10	6.5×10^{10}	12.1
D9	1.5 (unheated)	60	10	6.5×10^{10}	11.8
D10	1.5 (unheated)	60	10	6.5×10^{10}	10.2
D11	1.5 (hot)	60	10	6.5×10^{10}	10.7

SDCV contains a considerable amount of water. Heating of SDCV inside the Knudsen reactor resulted in loss of 1.2 mg water per g of dust. Interestingly, it did not make a difference for the uptake coefficient if we heated the sample or not (experiments D9 and D10). Also even on hot SDCV (353 K; experiment D11), the uptake coefficient was as high as on dust at 298 K. This is explained by dehydration curves of clay minerals which show that substantial loss of water does not occur at temperatures below 673 K (illite) or 773 K (kaolinite, chlorite). For example, kaolinite loses 10% of its weight in the form of water by heating between 773 and 823 K.[31] The 1.2‰ weight loss after heating at 353 K as in the present experiments cannot be considered to represent a substantial loss of water and explains why uptake of HNO_3 is not influenced by the standard "drying" procedure.

Although no evidence for product formation from reactive uptake was observed, the irreversibility of the uptake process could be confirmed in the following experiment. After extended exposure to HNO_3, the dust sample was isolated from the Knudsen reactor (plunger closed) and the HNO_3 flow disabled. After the signal at m/e 46 had decreased to about 5% of its steady-state flow value, the plunger was lifted. The absence of an increase in the HNO_3 signal was taken to confirm that desorption of physisorbed HNO_3 from the surface was insignificant.

3.6. Role of Internal Surface Area in Calculation of γ_{init}. In section 3.1, we briefly addressed the role of pore diffusion for calculation of the uptake coefficient. If pore diffusion is significant on the time scale of the measurement of the initial uptake coefficient, this parameter, defined in the following as γ_{init}^{geom}, should be corrected for the internal surface area. In this

TABLE 6: Comparison of Uncorrected and Corrected Uptake Coefficients on Al_2O_3

average grain size (μm)	γ_{init}^{geom}	γ^{BET}	γ^{pd}
2.4	12.6×10^{-2}	2.2×10^{-4}	16×10^{-4}
27	(8.2×10^{-2})		
59	13.2×10^{-2}	11×10^{-4}	12×10^{-4}
112	13.4×10^{-2}	34×10^{-4}	34×10^{-4}

section, we compare the uncorrected (i.e., geometric) uptake coefficients for Al_2O_3 (expts A23−A26) to the corrected ones, taking into account the four particle size classes, and explain why we think that no correction is needed for uptake experiments with HNO_3.

A simple correction method is to use the BET area of a sample instead of the geometrical surface area:

$$\gamma^{BET} = \frac{A^{geom}}{A^{BET}} \gamma_{init}^{geom} \qquad \text{(ix)}$$

where A^{geom} is the geometrical surface area of the sample (1.5 cm^2), $\gamma_{init}^{geom} = 13 \times 10^{-2}$, and A^{BET} is the BET surface area of the sample, calculated for the sample mass of 60 mg using the specific BET areas given in section 3.1 and Table 2. Calculated values for γ^{BET} are presented in Table 6.

A more sophisticated correction method which takes into consideration the relative rate of surface reaction and pore diffusion effects has been presented by Keyser and coworkers.[32−34] This method was originally developed for heterogeneous reactions on vapor deposited ice surfaces but has also been applied to reactions on granular surfaces. To take into account the porosity of the Al_2O_3 grains bigger than 10 μm, we calculated the correction for pore diffusion according to Keyser et al.[34]

$$\gamma_{init}^{geom} = \gamma^{pd} \rho_b A^{BET} \bar{d} \left(\frac{1}{2} + \eta \left(\frac{h}{\bar{d}} - \frac{1}{2} \right) \right) \qquad \text{(x)}$$

where η is the "effectiveness" factor, $\eta = (\tanh \phi)/\phi$, and ϕ is the Thiele modulus whereby

$$\phi = \left(\frac{h}{\bar{d}} - \frac{1}{2} \right) \frac{3\rho_b}{2(\rho_t - \rho_b)} \sqrt{3\tau\gamma^{pd}} \qquad \text{(xi)}$$

The input parameters for the calculation of the pore diffusion-corrected uptake coefficient γ^{pd} are the uncorrected uptake coefficient γ_{init}^{geom}, the total height of the Al_2O_3 sample h ($h = h_i + h_e$, where h_i and h_e are the internal and external thickness of the substrate), the average grain size of the Al_2O_3 particles $\bar{d}$, the true density of crystalline Al_2O_3 ρ_t (= 3.97 g/cm^3), the bulk density of the Al_2O_3 sample ρ_b, and the tortuosity factor τ. The sample heights were between 420 μm (for $d < 10$ μm) and 210 μm (for 74 μm $< d <$ 149 μm), resulting in bulk densities of between 0.9 and 1.8 g/cm^3, respectively. On the basis of inspection of the SEM micrographs, we determined $\bar{d} = 2.4$ μm for grain class 1, and for the other classes, we took the arithmetic mean of the respective upper and lower size limits. The tortuosity factor was set to $\tau = 2$, following calculations for HNO_3 on NaCl grains.[35] Our calculated values for γ^{pd} are listed in Table 6.

Values of γ^{BET} and of γ^{pd} are 2 to 3 orders of magnitude lower than uncorrected γ values and, with the exception of the smallest grain size, are in good agreement with each other. This agreement shows that, if the pore diffusion model were applicable, the data should lay in the linear mass-dependent region as defined by Underwood et al,[36] where the relevant surface area is the total external and internal surface area. As already pointed out in section 3.1, the constancy of γ_{init}^{geom} with varying grain size is a strong indication that the internal surface of the sample is not of great significance for the HNO_3 uptake. If the pore diffusion correction were applicable to HNO_3, the values of γ_{init} for the experiments with HNO_3 on 30, 60, and 100 mg of Al_2O_3 (74 μm $< \bar{d} <$ 149 μm; expts A9, A13, and A20−A22) should display a linear dependence on sample mass; the independence of γ_{init} upon changing the sample mass suggests this is not the case. In the insert to Figure 4, we plot values of γ_{init} obtained under identical conditions (initial HNO_3 concentration, grain size, etc.), except that the sample mass was varied. The solid lines are the result of a pore diffusion calculation for uptake onto this substrate. Despite variation of τ over a broad range (2−20), the model was not able to reproduce the (lack of) dependence of the initial uptake coefficient on sample mass.

The nonapplicability of the pore diffusion model is further corroborated by the results for γ^{BET} and γ^{pd} which show a strong dependency on grain size. In contrast, Caloz et al.[37] were able to align uptake coefficients for $ClNO_2$ on KBr that varied over 2 orders of magnitude by applying the correction for pore diffusion. In our study, the opposite is the case, and initially consistent data are converted to uptake coefficients that vary over a factor of 3.

Strictly speaking, the fact that we did not observe a dependence of γ on grain size for Al_2O_3 does not prove the assumption that the other substrates used in this study behave in the same manner. However, together with the results for HNO_3 onto $CaCO_3$ (Fenter et al.[29]) and for HNO_3 onto NaCl and KBr, our assertion that sample surface presentation has no influence on the initial uptake of HNO_3 appears justified.

In equations x and xi, the Thiele modulus ϕ is a measure of the surface reaction rate to the porous diffusion rate. If diffusion does not play a role with respect to surface reaction, ϕ must become very large. As a consequence, η approaches zero and eq x reduces to

$$\gamma_{init}^{geom} = \gamma^{pd} \rho_b A^{BET} 0.5 \bar{d} \qquad \text{(xii)}$$

With this formula we calculated corrected γ values of 8×10^{-2} for grains with $d < 10$ μm and 1.4×10^{-2} for the other sizes. The result for the smallest grains is expected to be the most accurate because the porous nature of individual larger grains (which themselves are aggregates of smaller particles, see Figure 3) precludes accurate estimation of $\bar{d}$.

We therefore conclude that neither the simple BET correction nor the pore diffusion correction are appropriate for the uptake experiments with HNO_3. A correction for surface enlargement due to the roughness of the surface (equation xii) may be appropriate and would result in a reduction of the initial uptake coefficients by a factor of about 2.

3.7. Comparison with Literature. Laboratory investigations of the interaction of HNO_3 with any of the surfaces used in the present study are limited in number. For comparison with literature data, we use the uncorrected initial uptake coefficients based on the geometric surface area, which is generally the reported quantity.

Our results for the uptake of HNO_3 onto $CaCO_3$ are in excellent agreement with a previous Knudsen reactor investigation[29] in which an uptake coefficient of $\gamma = (10 \pm 2) \times 10^{-2}$ was obtained. For damp $CaCO_3$, the uptake coefficients from

experiments B10 ($\gamma = 14 \times 10^{-2}$) and B16 ($\gamma = 18 \times 10^{-2}$) are also in excellent agreement with previous measurements[29] on damp $CaCO_3$ pellets, in which an uptake coefficient of $\gamma = (15 \pm 3) \times 10^{-2}$ was determined. Another Knudsen reactor study for HNO_3 onto $CaCO_3$[36] found uptake coefficients between 2.3×10^{-3} and 4×10^{-4}, depending on the sample mass. These uptake coefficients are ca. 2 orders of magnitude lower than the present values and those obtained by Fenter et al.[29] The reason for this discrepancy is unclear.

The reaction of HNO_3 with a dry Na_2CO_3 surface has also been investigated using a Knudsen reactor[29] and an annular reactor[38] to obtain uptake coefficients of 7.6×10^{-2} and 1.5×10^{-2}, respectively. Further evidence for the reaction of HNO_3 on mineral particles is provided by the work of Mamane and Gottlieb,[39] who used electron microscopic and bulk analysis techniques to observe and quantify nitrate formation on single particles that were exposed to 0.04 ppm HNO_3 under conditions similar to ambient (70% humidity at room temperature). They found that ≈30 mg nitrate per g of aerosol were formed under favorable conditions. Although the data on the reactivity of HNO_3 to mineral oxide and mineral dust surfaces is still very limited, observations of gas uptake and nitrate formation provide strong evidence for an efficient reactive uptake process.

3.8. Atmospheric Implications. The atmospheric implications of the present results are assessed by taking the Saharan dust sample used in the laboratory to be mineralogically representative of atmospheric dust aerosol. The mineralogical composition of SDCV that we used has been described in the literature (e.g., see ref 40) and closely simulates atmospheric particles of crustal origin.[41] The clay fraction (<2 μm) of dust from Cape Verde shows a kaolinite−illite−chlorite assemblage which is typical for central Saharan dust, though the predominance of illite and kaolinite is characteristic of dusts in other regions of the world.

We note that our experimental set up does not allow one potentially important parameter, the humidity of the sample, to be varied over an appropriate range. We have however shown that the reactivity of the Saharan dust sample is not influenced by strong heating and that the reactivity of $CaCO_3$ is slightly increased by the presence of H_2O vapor. The fact that large uptake coefficients were obtained for the "dry" conditions of the Knudsen reactor experiments, where the relative humidity is orders of magnitude less than that observed anywhere in the lower troposphere, suggests that an uptake coefficient of 0.1 (taken from the data on Saharan dust) may be considered a conservative estimate of the true uptake coefficient. The greatest effect of humidity is expected to be related to the capacity of the dust to remove HNO_3.

The rate of removal of HNO_3 by uptake onto mineral dust can be approximated in a simple model, which assumes spherical geometry for particles and thus underestimates the surface area density. We assume that the lifetime τ for removal of HNO_3 by dust is given by

$$\tau = \frac{4}{\gamma \bar{c} A} \qquad \text{(xiii)}$$

where A is the dust surface area density in cm^2/cm^3. If we assume a conservatively low (i.e., background) dust loading of 5 $\mu g/m^3$, we obtain $A \approx 10^{-7}$ cm^2/cm^3. Our measured uptake coefficient $\gamma = 0.1$ then leads to a HNO_3 lifetime with respect to processing by dust of ≈4 h. This is considerably shorter than the gas phase photochemical lifetime due to reaction with OH and photolysis which is ≈300 h in the lower troposphere. In addition, field observations have shown that up to 10% of the aerosol mass (or 75% of the calcite content) can be converted to nitrate. This implies that 5 $\mu g/m^3$ can remove a total of 0.5 μg HNO_3 which is equivalent to ≈200 ppt at the earth's surface.

This simple calculation is very crude in nature but indicates that interaction with mineral dust may be an important loss process for tropospheric HNO_3 and shows why modeling studies of mineral dust interactions with HNO_3 have revealed an important role for this process.

4. Conclusions

We have determined the uptake coefficient for the reaction of HNO_3 with authentic mineral dust samples for the first time. A value of $\gamma = 11 \times 10^{-2}$ was determined for SDCV at 298 K. The result for ATD was $\gamma = 6 \times 10^{-2}$. Measurements of the uptake coefficient of HNO_3 on Al_2O_3 ($\gamma = 13 \times 10^{-2}$) enabled us to show that the geometrical surface area of the dust sample is most appropriate for calculation of the uptake coefficients in this study. The uptake coefficients for HNO_3 on dry $CaCO_3$ and on damp $CaCO_3$ are given by $\gamma = 10 \times 10^{-2}$ and 18×10^{-2}, respectively, and are in good agreement with previous results.[29] The reaction was found to be sensitive to the amount of surface-adsorbed water. Experiments with HNO_3 on single crystals ($\gamma \approx 10^{-3}$) showed that the lack of surface defects results in a reduction of the uptake coefficient. Our results indicate a generally very high reactivity of HNO_3 toward dust samples, highlighting the potentially important role of mineral dust in modifying the distribution of nitrate between the gaseous and particulate phases.

Acknowledgment. We gratefully acknowledge L. Gomes for supplying the Cape Verde loess sample and D. Levi (Du Pont) for provision of the FEP 121-A Teflon suspension used to coat the Knudsen reactor. Thanks are due to Cedric du Fresne and Joachim Huth for conducting the BET and the SEM measurements, respectively. We acknowledge partial funding from the BMBF (AFS-07AF210B8) and the German−Israeli Foundation for Scientific Research and Development (I156-303.06/97).

References and Notes

(1) Tegen, I.; Fung, I. *J. Geophys. Res.* **1994**, *99*, 22897.
(2) Carmichael, G. R.; Zhang, Y.; Chen, L.-L.; Hong, M.-S.; Ueda, H. *Atmos. Environ.* **1996**, *30*, 2407.
(3) Li, X.; Maring, H.; Savoie, D.; Voss, K.; Prospero, J. M. *Nature* **1996**, *380*, 416.
(4) Prospero, J. M. *Proc. Natl. Acad. Sci. U.S.A.* **1999**, *96*, 3396.
(5) Savoie, D. L.; Prospero, J. M. *Geophys. Res. Lett.* **1982**, *9*, 1207.
(6) Duce, R. A.; Unni, C. K.; Ray, B. J.; Prospero, J. M.; Merrill, J. T. *Science* **1980**, *209*, 1522.
(7) Chester, R. *Sci. Geol. Mem.* **1990**, *88*, 23.
(8) Gomes, L.; Gillette, D. A. *Atmos. Environ.* **1993**, *27A*, 2539.
(9) Zhang, Y.; Sunwoo, Y.; Kotamarthi, V.; Carmichael, G. R. *J. Appl. Met.* **1994**, *33*, 813.
(10) Dentener, F. J.; Carmichael, G. R.; Zhang, Y.; Lelieveld, J.; Crutzen, P. J. *J. Geophys. Res.* **1996**, *101*, 22869.
(11) Chatfield, R. B. *Geophys. Res. Lett.* **1994**, *21*, 2705.
(12) Hauglustaine, D. A.; Ridley, B. A.; Solomon, S.; Hess, P. G.; Madronich, S. *Geophys. Res. Lett.* **1996**, *23*, 2609.
(13) Jacob, D. J.; Heikes, B. G.; Fan, S.-M.; Logan, J. A.; Mauzerall, D. L.; Bradshaw, J. D.; Singh, H. B.; Gregory, G. L.; Talbot, R. W.; Blake, D. R.; Sachse, G. W. *J. Geophys. Res.* **1996**, *101*, 24235.
(14) Ridley, B.; Walega, J.; Huebler, G.; Montzka, D.; Atlas, E.; Hauglustaine, D.; Grahek, F.; Lind, J.; Campos, T.; Norton, R.; Greenberg, J.; Schauffler, S.; Oltmans, S.; Whittlestone, S. *J. Geophys. Res.* **1998**, *103*, 8323.
(15) Thakur, A. N.; Singh, H. B.; Mariani, P.; Chen, Y.; Wang, Y.; Jacob, D. J.; Brasseur, G.; Müller, J.-F.; Lawrence, M. *Atmos. Environ.* **1999**, *33*, 1403.
(16) Nishikawa, M.; Kanamori, S. *Anal. Sci.* **1991**, *7*, 1127.

(17) Okada, K.; Naruse, H.; Tanaka, T.; Nemoto, O.; Iwasaka, Y.; Wu, P.-M.; Ono, A.; Duce, R. A.; Uematsu, M.; Merrill, J. T. *Atmos. Environ.* **1990**, *24A*, 1369.
(18) Savoie, D. L.; Prospero, J. M. *Nature* **1989**, *339*, 685.
(19) Prospero, J. M.; Savoie, D. L. *Nature* **1989**, *339*, 687.
(20) Savoie, D. L.; Prospero, J. M.; Nees, R. T. *Geophys. Res. Lett.* **1987**, *92*, 933.
(21) Wolff, G. T. *Atmos. Environ.* **1984**, *18*, 977.
(22) Mamane, Y.; Ganor, E.; Donagi, A. E. *Water, Air, Soil Pollut.* **1980**, *14*, 29.
(23) Loyë-Pilot, M. D.; Martin, J. M.; Morelli, J. *Nature* **1986**, *321*, 427.
(24) Rognon, P.; Coudé-Gaussen, G.; Revel, M.; Grousset, F. E.; Pedemay, P. *Sedimentology* **1996**, *43*, 359.
(25) Beichert, P.; Finlayson-Pitts, B. J. *J. Phys. Chem.* **1996**, *100*, 15218.
(26) Allen, H. C.; Laux, J. M.; Vogt, R.; Finlayson-Pitts, B. J.; Hemminger, J. C. *J. Phys. Chem.* **1996**, *100*, 6371.
(27) Ghosal, S.; Hemminger, J. C. *J. Phys. Chem. A* **1999**, *103*, 4777.
(28) Davies, J. A.; Cox, R. A. *J. Phys. Chem.* **1998**, *102*, 7631.
(29) Fenter, F. F.; Caloz, F.; Rossi, M. J. *Atmos. Environ.* **1995**, *29*, 3365.
(30) Fenter, F. F.; Caloz, F.; Rossi, M. J. *J. Phys. Chem.* **1994**, *98*, 9801.
(31) Grim, R. E. *Clay Mineralogy*; McGraw-Hill: New York, 1953.
(32) Keyser, L. F.; Moore, S. B.; Leu, M. T. *J. Phys. Chem.* **1991**, *95*, 5496.
(33) Keyser, L. F.; Leu, M.-T. *J. Colloid Interface Sci.* **1993**, *155*, 137.
(34) Keyser, L. F.; Leu, M.-T.; Moore, S. B. *J. Phys. Chem.* **1993**, *97*, 2800.
(35) Leu, M. T.; Timonen, R. S.; Keyser, L. F.; Yung, Y. L. *J. Phys. Chem.* **1995**, *99*, 13203.
(36) Underwood, G. M.; Li, P.; Usher, C. R.; Grassian, V. H. *J. Phys. Chem. A* **2000**, *104*, 819.
(37) Caloz, F.; Seisel, S.; Fenter, F. F.; Rossi, M. J. *J. Phys. Chem.* **1998**, *38*, 7470.
(38) Msibi, I. M.; Shi, J. P.; Harrison, R. M. *J. Atmos. Chem.* **1993**, *17*, 339.
(39) Mamane, Y.; Gottlieb, J. *J. Aerosol Sci. Technol.* **1990**, *21*, 225.
(40) Coudé-Gaussen, G.; Rognon, P.; Le Coustumer, M. C. *R. Acad. Sci.* **1994**, *319*, 1343.
(41) Desboeufs, K. V.; Losno, R.; Vimeux, F.; Cholbi, S. *J. Geophys. Res.* **1999**, *104*, 21287.